

CHAPTER 15

Modelling Post-Wave Breaking Turbulence and Vorticity.

T.C.D.Barnes, M.Brocchini,[†] D.H.Peregrine[‡] and P.K.Stansby[§]

1. Abstract

A brief review is given of the initial development of two approaches to the modelling of the flow that occurs after a water wave breaks. The first approach aims to model the turbulence generated by a spilling breaker riding on an unsteady wave. The turbulent volume of water in a spiller is modelled as a thin layer.

The second approach is applied to model the region of strong vorticity generated by a plunging breaker. The vorticity is modelled using two-dimensional discrete vortices. The behaviour of both a single vortex and a ‘cloud’ of vortices near a free surface is described.

2. Introduction

Water wave breakers, whether in deep or shallow water are mainly categorized as spilling or plunging breakers with no clear distinction between them. In particular intermediate types certainly exist, where there is a small initial plunging event which initiates tumbling white water as in a spiller. The strongly vortical and turbulent flow which results from all types of breaker is the interest of our studies. We distinguish between the turbulence and the vorticity of the mean flow. For example, a plunging breaker frequently creates a strong vortical flow about a horizontal axis. First steps in using discrete vortices in a two-dimensional model with a fully nonlinear free surface are described in the second part of this paper. The first section describes the modelling of a thin layer of turbulence in a spilling breaker.

[†]Research assistants, School of Mathematics, University of Bristol, University Walk, Bristol, BS8 1TW, UK, (*Tim.Barnes@bristol.ac.uk*, *M.Brocchini@bristol.ac.uk*)

[‡]Professor of Applied Mathematics, School of Mathematics, University of Bristol, (*D.H.Peregrine@bristol.ac.uk*)

[§]Professor of Civil Engineering, Department of Engineering, University of Manchester. (*pkstansby@fs1.eng.man.ac.uk*)

3. Turbulence and vorticity in a spilling breaking wave

In their analysis of spilling breakers, bores and hydraulic jumps Peregrine & Svendsen (1978) suggested that the volume of turbulent flow in a spilling breaker resembles a turbulent mixing layer. The roller model in which the turbulent region is modeled as a separate flow region passively riding the wave crest is seen to be only a partial solution as it is evident that the fluid content of the roller itself is continually mixing with the rest of the turbulent fluid in the wave.

Peregrine (1992) also suggests that a spilling breaker may be considered as a quasi-steady system in a frame of reference moving with the wave where deformations of the spiller shape occur at longer time scales than those typical of the motion of water through the turbulent region. The structure of such a quasi-steady breaker is thus an initial mixing layer region, followed by a region beneath the crest of the wave where gravity influences and restrains the turbulent motions near the surface.

This view leads to consideration of a turbulent layer where turbulence is generated at the leading edge (toe of the wave) by shear stresses due to the relative motion between the turbulent wave surface and the water in which the wave propagates. Turbulence, generated near the free surface, propagates within the body of the wave and the turbulent layer evolves from a mixing layer type flow near the leading edge towards a wake type flow where most of the turbulent kinetic energy is dissipated.

This scenario is now documented for a small, quasi-steady spilling breaker, a recent experimental analysis of which is given by Lin & Rockwell (1995). It is found that the breaker originates from a region where the free surface abruptly changes slope (toe of the wave). The magnitude of the velocity is virtually unaltered until the abrupt onset of curvature of the free surface is encountered. At this location, there is a drastic nearly discontinuous reduction in magnitude of the velocity. The change in the velocity field is accompanied by a sudden increase in elevation of the free surface and represents an abrupt transformation from an undisturbed, essentially uniform velocity field to a very low velocity separated region existing beneath the free surface. The essentially discontinuous slope of the surface, in the presence of flow separation beneath it, serves as a source of vorticity giving rise to vorticity concentrations in a separated mixing layer, or shear layer.

We report on modelling of an unsteady thin turbulent layer (to be used in the modelling of a spilling breaking wave). One of the main assumptions is that the vertical extent of turbulent flow is much smaller than its streamwise extent. The motion of the wave is to be modelled by any suitable model for irrotational flows (e.g. boundary integral method) while the turbulent region of the breaker is modelled by a simplified $k - \epsilon$ model for a thin layer of fluid similar to that of Madsen & Svendsen (1983). The main new features of the present model are concerned with the correct representation of stretching, curvature, acceleration and local rotation that the layer of turbulent flow undergoes. Particular care has been put in analyzing the effects of curvature on the turbulent flow in the thin layer.

In figure 1 the global geometry of the present model for a spilling breaking wave is shown. Two regions of turbulent flow are identified. The 'surface layer'

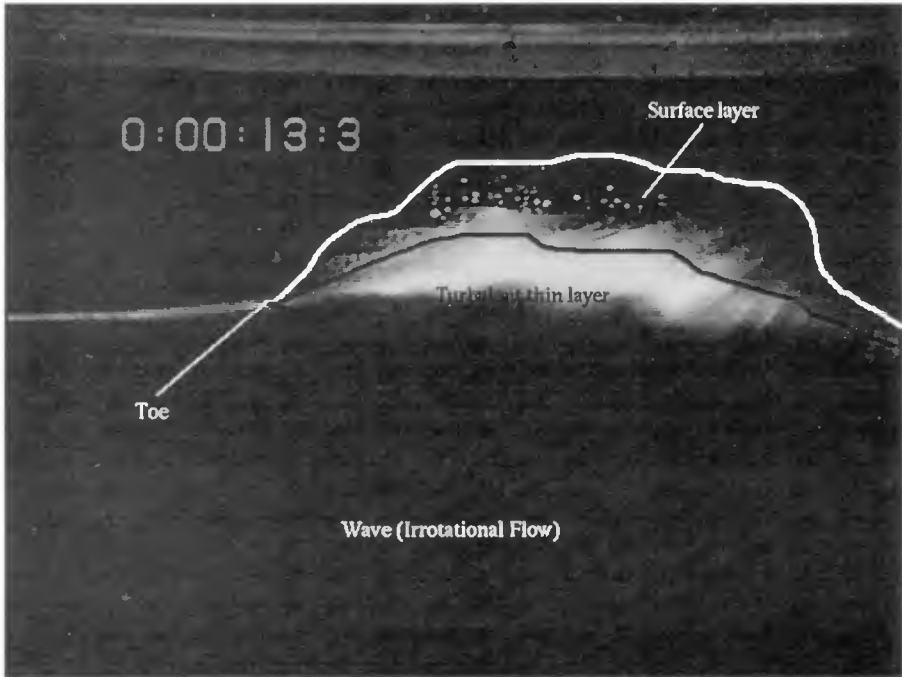


Figure 1: Global geometry adopted in the model for the system wave - turbulent thin layer - surface layer. Frame of video taken at the Fluid Dynamics unit of the University of Edinburgh.

region represents that portion of the turbulent thin layer where the instantaneous free surface fluctuates around the mean free surface. When turbulent eddies cause the interface to splash into the air phase a situation occurs in which space is occupied by two substances which have different properties (e.g. air and water) and can be distinguished from each other (Brocchini & Peregrine, 1997a). Thus, the flow is essentially a two-phase flow. Beneath the 'surface layer' a second layer is found where the flow is still turbulent but single-phase (water). A summary on the modelling of the single-phase turbulent thin layer follows.

Brocchini & Peregrine (1997a) analyses in detail the boundary conditions for a turbulent air-water mixture ('surface layer') occurring at a splashing free surface. In order to obtain conditioned equations for each phase (i.e. air and water) a phase function or intermittency function is introduced such that

$$I(\mathbf{x}, t) = \begin{cases} 1 & \text{probe at } \mathbf{x} \text{ is in the water at time } t \\ 0 & \text{probe at } \mathbf{x} \text{ is in the air at time } t. \end{cases} \quad (1)$$

An integral method has been used to assess the flow equation for the water phase. Exact boundary conditions have been obtained by integrating in the crossflow direction the equations for the water flow. These boundary conditions are com-

plicated and cannot be directly used in simple turbulence models (e.g. $k - \varepsilon$) because they are written in terms of the flow properties in the water phase rather than in terms of the ordinary mean flow variables. Approximations and closure assumptions are made to obtain simpler approximate boundary conditions for use in the modelling of the spilling breaker. The intermittency factor

$$\langle I(\mathbf{x}, t) \rangle = \gamma(\mathbf{x}, t) \quad (2)$$

is the ensemble average of $I(\mathbf{x}, t)$ and is the most important statistical parameter to characterize a specific surface layer. Thus, closure is based on a suitable definition for γ for each flow regime (see figure 2).

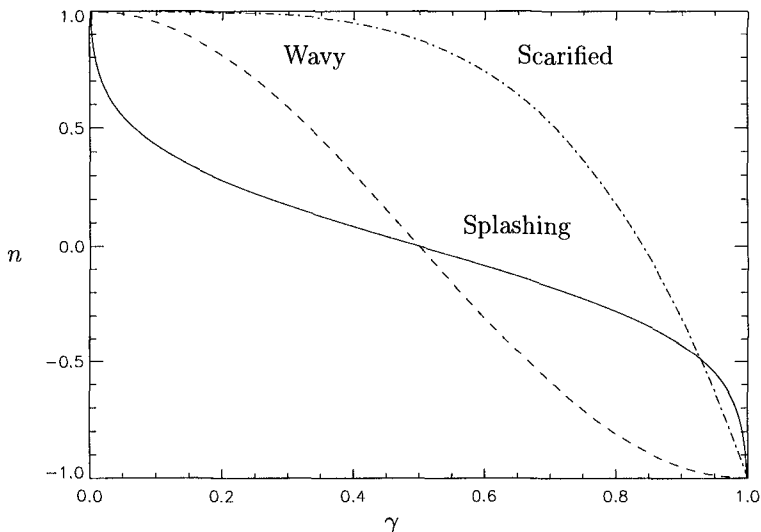


Figure 2: The intermittency factor (or residence time) γ for: (a) wavy air-water interface (dashed line), (b) periodically scarified interface (dot-dashed line) and (c) turbulent splashing interface (solid line).

Since the main aim of the modelling is to correctly represent the stretching, curvature, acceleration and local rotation that the layer of turbulent flow undergoes we use the tools of curvilinear tensor analysis to derive the flow equations and derive a more general version of Svendsen & Madsen, (1984) thin, hydrostatic layer for a shallow water flow. Here the underlying irrotational wave motion is supposed to be modelled by an accurate flow solver, such as that of Dold & Peregrine (1986), modified to use the following thin layer equations as a boundary condition.

We start from Euler's equation for a Newtonian, incompressible, perfect fluid

of constant density ρ :

$$\rho \frac{Du_i}{Dt} = \rho F_i - p_{,j}. \quad (3)$$

where the comma refers to partial covariant differentiation. The left hand side of this equation contains the total derivative of the flow velocity. The two contributions on the right hand side are due to the external forces (here only gravity) and to the pressure p . A set of two-dimensional orthogonal coordinates (ξ_1, ξ_2) is defined as follows (Moore, 1978).

Consider a smooth time-dependent two-dimensional curve $\Upsilon(t)$ (see Figure 3) given parametrically by the equation

$$\mathbf{r} = \mathbf{R}(\alpha, t) \quad (4)$$

where t is time and α is an arbitrary parameter. The curve $\Upsilon(t)$ represents either the wave free surface when no breaking occurs or an interface between the irrotational flow region (below) and the region containing turbulent flow (above). Due to the typical entrainment of irrotational flow into the region of turbulence the curve $\Upsilon(t)$ is not a material surface when turbulence is present, i.e. water particles which at time $t = t_0$ are on the surface $\Upsilon(t)$ at a later time $t = t_1$ will not be on the surface any more.

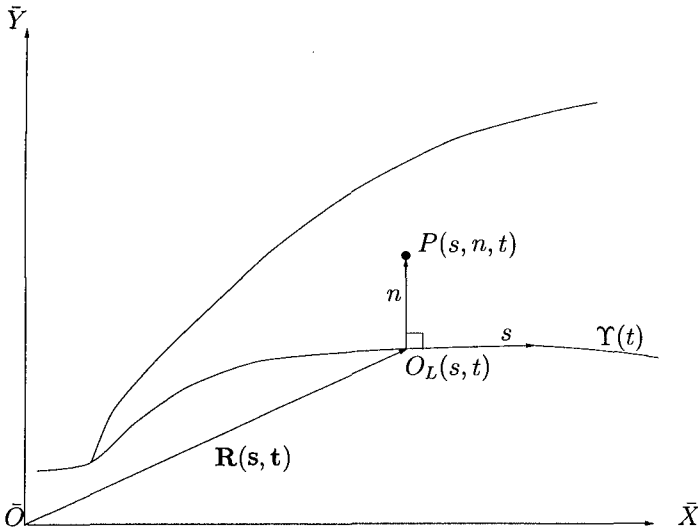


Figure 3: Definitions for geometry and coordinates used for the thin turbulent layer.

With each "convected point" $O_L(\alpha(s), t)$ of the curve we associate a unit tangent vector $\hat{\mathbf{s}}(\alpha(s), t)$ to the curve defined by

$$\hat{\mathbf{s}} = \frac{\partial \mathbf{R}}{\partial s} \quad \text{so} \quad \frac{\partial \mathbf{R}}{\partial \alpha} = \frac{\partial s}{\partial \alpha} \frac{\partial \mathbf{R}}{\partial s} = \frac{\partial s}{\partial \alpha} \hat{\mathbf{s}}; \quad (5)$$

and also a unit normal vector $\hat{\mathbf{n}}(\alpha(s), t)$. For the sake of simplicity much of the following analysis is carried out by referring differential quantities to the arc length s rather than to the convected coordinate α , hence the position of each convected point $O_L(s, t)$ in the fixed frame of reference $\bar{O}\bar{X}\bar{Y}$ is:

$$\mathbf{r} = \mathbf{R}(s, t). \quad (6)$$

For any general point P , which is in the turbulent layer (i.e. above Υ) we assume that it is close enough to Υ that there is only one normal to the curve passing through O_L towards P and the distance $O_L P = n$ is also defined. This is positive if P is on the left hand side of Υ when this is described in the s -increasing direction (i.e. above Υ). Moreover the position of the point P within the thin layer is determined by two coordinates $\xi^1 = s$, $\xi^2 = n$ which form a mobile curvilinear coordinate system.

With this convention the position of P in $\bar{O}\bar{X}\bar{Y}$ is :

$$\mathbf{r}_P(s, n, t) = \mathbf{R}(s, t) + \hat{\mathbf{n}}(s, t)n. \quad (7)$$

The metric tensor g_{ij}^M can be identified more clearly by analysing the infinitesimal distance between two points P and Q and is:

$$ds^2 = d\mathbf{r} \cdot d\mathbf{r} = (1 - \kappa n)^2 ds^2 + dn^2 = g_{ij}^M d\xi_i d\xi_j. \quad (8)$$

where κ is the local curvature.

The model comprises four equations for the mean flow. Mean flow variables are in capital letters (e.g. U, V, P) while turbulent fluctuations are in lower case (e.g. u, v). A first equation states the conservation of mass:

$$\frac{\partial U}{\partial s} + \frac{\partial}{\partial n} [(1 - \kappa n)V] = n \frac{\partial \Omega}{\partial s}. \quad (9)$$

Here two extra terms due to the angular velocity Ω and to the curvature κ influence the mean motion.

The two equations for the conservation of momentum in the streamwise and crossflow direction are respectively:

$$(1 - \kappa n) \frac{\partial U}{\partial t} + (1 - \kappa n) \left[\left(V + \hat{\mathbf{n}} \cdot \frac{\partial \mathbf{R}}{\partial t} \right) \frac{\partial U}{\partial n} + \frac{\partial \langle uv \rangle}{\partial n} \right] + \frac{\partial \langle u^2 \rangle}{\partial s} - 2\kappa \langle uv \rangle \quad (10)$$

$$+ \left(U + \hat{\mathbf{s}} \cdot \frac{\partial \mathbf{R}}{\partial t} - n\Omega \right) \left(\frac{\partial U}{\partial s} - n \frac{\partial \Omega}{\partial s} - \kappa V \right) = (1 - \kappa n) \left(V\Omega + \frac{\partial (n\Omega)}{\partial t} + \hat{\mathbf{s}} \cdot \mathbf{g}' \right) - \frac{1}{\rho} \frac{\partial P}{\partial s},$$

and

$$\frac{\partial V}{\partial t} + \hat{\mathbf{n}} \cdot \frac{\partial \mathbf{R}}{\partial t} \frac{\partial V}{\partial n} + \frac{1}{2} \frac{\partial V^2}{\partial n} + \frac{\partial \langle v^2 \rangle}{\partial n} + \frac{1}{(1 - \kappa n)} \hat{\mathbf{s}} \cdot \frac{\partial \mathbf{R}}{\partial t} \left(\frac{\partial V}{\partial s} + \kappa U \right) + \frac{(U - n\Omega)}{(1 - \kappa n)} \left(\frac{\partial V}{\partial s} + \kappa U \right)$$

$$+ \frac{1}{(1 - \kappa n)} \frac{\partial \langle uv \rangle}{\partial s} + \frac{\kappa \langle u^2 \rangle - \langle v^2 \rangle}{(1 - \kappa n)} = n\Omega^2 - U\Omega + \hat{\mathbf{n}} \cdot \mathbf{g}' - \frac{1}{\rho} \frac{\partial P}{\partial n}. \quad (11)$$

where $\langle \cdot \rangle$ is the average operator and \mathbf{g}' is the 'reduced' gravity factor

$$\mathbf{g}' = \mathbf{g} - \frac{\partial^2 \mathbf{R}}{\partial t^2}. \quad (12)$$

The above are the Reynolds' equations for our two-dimensional mean flow. As usual Reynolds' decomposition of non-linear convective terms introduces Reynolds' stress terms $\langle u_i u_j \rangle$ and isolates the effects of fluctuations on the mean flow.

These equations resemble the equations used in the modelling of a curved thin layer of turbulence (e.g. Gibson & Rodi, 1981). One of the main differences is that in the present case there is interactive coupling (through $\partial \mathbf{R} / \partial t$ and \mathbf{g}') between the motion of the thin layer of turbulence and that of the irrotational wave below.

Finally, modelling of the turbulence may be achieved by means of a simplified $k - \varepsilon$ model in which a first order closure is adopted such that we only solve a transport equations for the turbulent kinetic energy k :

$$\begin{aligned} \frac{\partial k}{\partial t} + \frac{1}{(1 - \kappa n)} \left(U + \hat{\mathbf{s}} \cdot \frac{\partial \mathbf{R}}{\partial t} - n\Omega \right) \frac{\partial k}{\partial s} + \left(V + \hat{\mathbf{n}} \cdot \frac{\partial \mathbf{R}}{\partial t} \right) \frac{\partial k}{\partial n} = \frac{1}{(1 - \kappa n)^2} \frac{\partial}{\partial s} \left(\nu_t \frac{\partial k}{\partial s} \right) \\ + \frac{\partial}{\partial n} \left(\nu_t \frac{\partial k}{\partial n} \right) + (\langle u^2 \rangle - \langle v^2 \rangle) \frac{\partial V}{\partial n} - \frac{\langle uv \rangle}{(1 - \kappa n)} \left[(1 - \kappa n) \frac{\partial U}{\partial n} + \frac{\partial V}{\partial s} + \kappa U \right] - \varepsilon. \end{aligned} \quad (13)$$

Here ε and ν_t are respectively the energy dissipation and the eddy viscosity such that:

$$\varepsilon \approx \frac{k^{3/2}}{\delta}, \quad \text{and} \quad \nu_t \approx \frac{k^2}{\varepsilon} \quad (14)$$

where δ is the thickness of the turbulent layer.

Modelling the dynamics of the thin layer of turbulence provides suitable boundary conditions for the irrotational flow of the wave. The turbulence/wave interaction occurring at lower boundary ($n = 0$) of the turbulent layer is represented by mass entrainment across the boundary and by extra pressure at the boundary. These extra terms are to be incorporated respectively in the kinematic and in the dynamic boundary condition for the irrotational wave along $\Upsilon(t)$. For example the kinematic boundary condition for the irrotational wave is:

$$\hat{\mathbf{s}} \cdot \frac{\partial \mathbf{R}}{\partial t} + \frac{\partial s}{\partial t} = \frac{1}{(1 - \kappa n)} \frac{\partial \phi}{\partial s}, \quad (15)$$

$$\hat{\mathbf{n}} \cdot \frac{\partial \mathbf{R}}{\partial t} = \frac{\partial \phi}{\partial n} + \mathcal{V} \quad (16)$$

where ϕ is the velocity potential for the irrotational flow and \mathcal{V} is the 'entrainment velocity' i.e. the velocity at which the turbulent layer entrains irrotational flow across the boundary $n = 0$. Increasing entrainment is such that the interface $\Upsilon(t)$ is lowered. The velocity \mathcal{V} is parameterized in terms of the local amount of turbulence in the thin layer.

We refer to Brocchini (1996) and Brocchini & Peregrine (1997b) for a detailed description of the derivation of the model equations.

4. Modelling of Waves and Concentrated Vorticity

For large organised vortical motions that are generated by plunging breakers, we add point vortices to the two-dimensional fully nonlinear free surface boundary integral solver for irrotational flow described by Cooker *et al* (1990). The numerical model solves the following equations, the usual equations for inviscid, incompressible and irrotational potential flow with the full nonlinear boundary conditions:

$$\begin{aligned}
 \nabla^2\Phi &= 0 && \text{in fluid} - \{\mathbf{x}_i^v\} \\
 \frac{D\mathbf{x}}{Dt} &= \nabla\Phi && \text{on free surface} \\
 \frac{D\Phi}{Dt} &= \frac{1}{2}|\nabla\Phi|^2 - gy && \text{on free surface} \\
 \frac{\partial\Phi}{\partial n} &= 0 && \text{on solid boundaries}
 \end{aligned}
 \tag{17}$$

where $\mathbf{x} = (x, y)$, $\Phi(\mathbf{x}, t)$ is the velocity potential and g is the acceleration due to gravity. The velocity potential, Φ is composed of a regular part ϕ_r and a singular part ϕ_s . The singular part is due to a system of point vortices, centres $\{\mathbf{x}_i^v\}$ while the regular part is due to the free surface. The potential due to a single point vortex is augmented by its images in both the bed ($y = -h$) and the line $y = h$ above the free surface, which gives the following expression

$$\begin{aligned}
 \phi_s &= \kappa(\tan^{-1}[\coth[s(x - x^v(t))]\tan[s(y - y^v(t))]] \\
 &\quad - \tan^{-1}[\coth[s(x - x^v(t))]\tan[s(y + y^v(t) + 2h)]])
 \end{aligned}
 \tag{18}$$

where $s = \pi/4h$, $(x^v(t), y^v(t))$ is the position of the point vortex and κ its strength. The extra images are helpful in giving a singular solution which decays rapidly in space. The circulation around the point vortex is then $\Gamma = 2\pi\kappa$, $\Gamma > 0$ denotes circulation in the counter-clockwise direction. We define a Froude number $Fr = \kappa/\sqrt{(gL^3)}$ where L is some characteristic length scale, usually the distance of a vortex from the free surface. The system is non-dimensionalised with g and L , all results presented are dimensionless.

Tong (1991) computed the evolution of a single point vortex as it interacted with a free surface. He used the two dimensional fully nonlinear free surface potential flow numerical solver which solves the equations shown to model the free surface deformation (Cooke *et al* 1990). A single point vortex modelling the effect of vorticity, moving under the effect of its images and the free surface. We have extended the method to include a system of point vortices in order to model the effect of larger regions of vorticity.

In the extended model each point vortex moves under the influence of the free surface, the other vortices and its images. The free surface moves under the

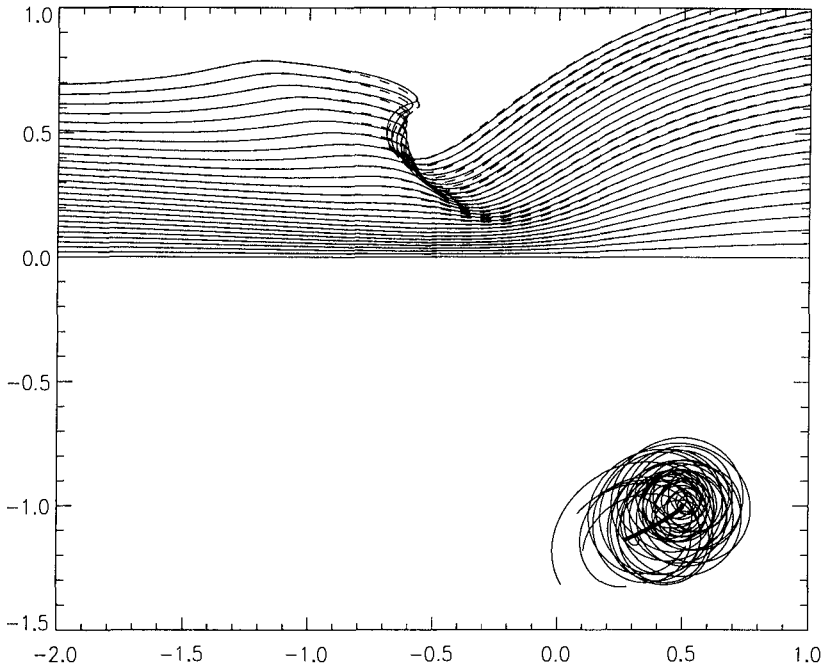


Figure 4: Stacked free surface deformation due to a single (solid) and 10 (dashed) vortices.

influence of the vortices and gravity. The numerical method which we use time-steps the free surface using a Taylor series expansion truncated at the sixth power of the time-step. The inclusion of the point vortices necessitates the computation of every partial derivative of the vortex potential in every combination of x , y and t up to the third derivative in order to maintain the accuracy of the scheme. The time step criterion must also be modified to include the vortices, as velocities are very high close to the singular core of a point vortex.

We present some preliminary results here: figure 4 shows the free surface deformation and vortex movement due to a single impulsively started vortex (dotted) with strength $\kappa = 0.5$ initial position $(0.5, -1)$, and due to a system of 10 vortices whose strengths are all constant, positive and sum to 0.5, initially grouped around $(0.5, -1)$.

We can see that the two cases are remarkably similar, and give us some hope that the point approximation can model patches of vorticity well. Clearly a very diffuse patch of vorticity will not be well modelled by a point vortex. Our model will allow us to define the limits within which a single point vortex is sufficient

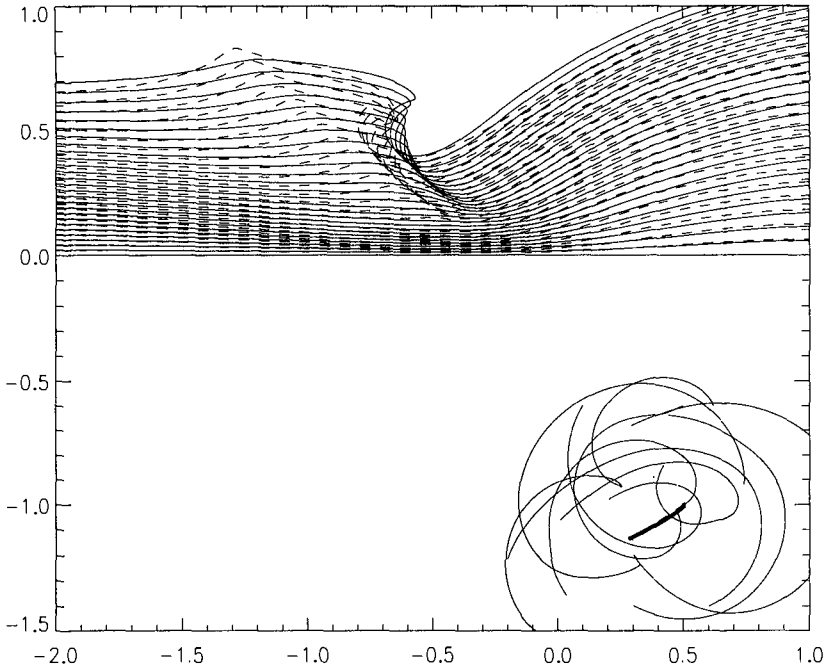


Figure 5: Stacked free surface deformation due to a single (solid) and 10 (dashed) vortices.

to model the free surface deformation due to a patch of vorticity.

We define the centre of the patch of vorticity to be the centroid of vorticity, the point defined by $\mathbf{X}_c^v = \frac{\sum_i \kappa_i \mathbf{x}_i^v}{\sum_i \kappa_i}$. Then the radius of the patch of vorticity is

defined as $R^v = \sqrt{\frac{\sum_i \kappa_i (\mathbf{x}_i^v - \mathbf{X}_c^v)^2}{\sum_i \kappa_i}}$. These definitions are also useful when defining centres and radii of patches of vorticity in experiments.

Figure 4 also shows the individual vortex paths. The thin lines are the paths of the system of 10 vortices, we can see that they co-rotate under their mutual influence, and drift under the influence of the free-surface. The thick line is the path of the single vortex and the centroid of the 10 vortices, which are virtually indistinguishable.

If the patch of vortices are sufficiently diffuse then there are variations from the behaviour in the single vortex case. Figure 5 shows such a case, where the free surface deformation is clearly different in the two cases. However similarities still exist, just outside the limits of the plot the free surface deformation is very

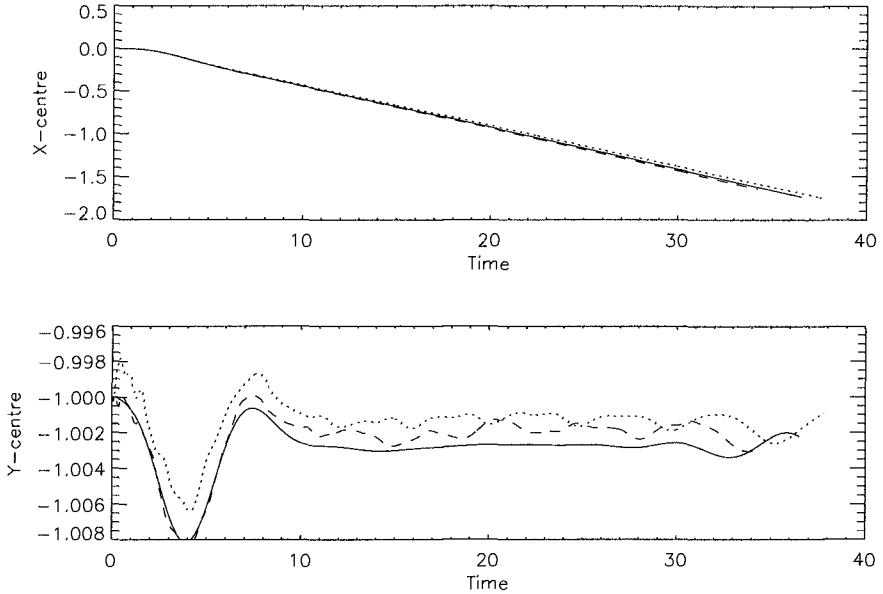


Figure 6: Path of single (solid), five (dashed) and ten (dotted) vortices sum strength 0.1

similar. Also the centre of the system of vortices and the single vortex still move along almost the same path, the thick line.

In certain cases the free surface deformation due to a patch of vorticity and a point vortex appear to be fairly similar. In such cases another interesting feature to study is the longer time evolution of a patch of vorticity which does not induce surface breaking. If the patch is modelled with a single point vortex then, for sufficiently weak vortices, the vortex moves as it would under a rigid wall. The image required to satisfy the rigid wall boundary condition predicts a vortex core velocity of $(-\kappa/2L, 0)$ for a point vortex located at $(x, -L)$. Individual point vortices in a patch of vorticity moving under the influence of the free surface alone will move with different velocities resulting in a diffusion of vorticity. So their interaction with each other and the free surface will determine the evolution of the patch of vorticity.

The solid line graphs in figure 6 show the paths of a single point vortex, strength $\kappa = 0.1$, initial position $(0, -1)$. After an initial transient period the vortex settles down to a constant x -velocity -0.049 with a small varying y -velocity, the rigid wall theory predicts a velocity of $(-0.05, 0)$. Note that the vortex takes some time to reach a steady state, initially sitting almost still. This is in qualitative agreement with the behaviour of vortices which we see in our

experiments (Quinn *et al* 1995 and Haydon *et al* 1996), which appear to take some time to start moving after being left by a plunging breaker.

The dotted and dashed path superimposed on figure 6 show the paths of the centres of systems of five and ten point vortices whose strengths sum to 0.1. We note that even the very small y -variations are fairly similar for all three cases. The radius of the patches is plotted in figure 7.

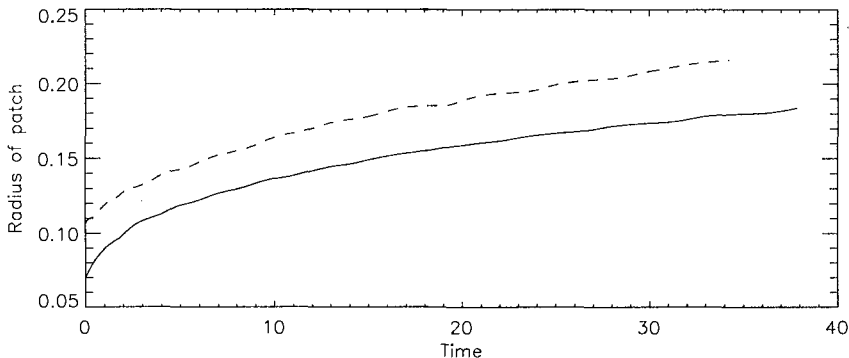


Figure 7: Radius of the patches in figure 6, five vortices (solid), ten vortices (dashed).

More importantly the free-surface generated in these three cases is also very similar, and rather complicated. It is also worth noting that the computations all fail at similar times due to a lack of points caused by a stretching of part of the free surface. This can be overcome by invoking a regridding procedure, we halt the computation at this point as it seems unlikely to yield any more interesting results.

Finally, we include the variation in the radius of the vortex cloud. Figure 7 shows the variation in the radius of the vortex clouds for the present example. We see that the cloud becomes steadily more diffuse, behaviour which is replicated in all cases which we have tried.

5. Conclusions

The work described in this paper continues. The thin layer model of a spilling breaker is being developed to add to boundary integral methods. The detailed analysis of the toe of the spiller is still in progress.

The discrete vortex system under a free surface is demonstrated to be practicable and may be of value for problems other than plunging breakers. For example the flows over many structures result in vortex shedding, which could be well described using the present methods.

6. Acknowledgments

Support from Engineering and Physical Sciences Research Council GR/J/43899 and GR/H/96836, European Union, Directorate General XII, contracts ERBCH-BICT930678 and MAS2-CT92-0047 is gratefully acknowledged.

7. References

- Brocchini, M. (1996). *Flows with freely moving boundaries: the swash zone and turbulence at a free surface*. Ph.D Dissertation. University of Bristol, Bristol.
- Brocchini, M. & Peregrine, D.H. (1997a). *The dynamics of a turbulent free surface. Part 2. The boundary conditions*. (in preparation).
- Brocchini, M. & Peregrine, D.H. (1997b) *The dynamics of a turbulent free surface. Part 3. A model for a spilling breaking wave*. (in preparation).
- Cooker, M.J., Peregrine, D.H., Vidal, C. and Dold, J.W. (1990) *The interaction between a solitary wave and a submerged semicircular cylinder*, J. Fluid Mech. **215**, 1-22.
- Dold, J.W. & Peregrine, D.H. (1984). *Steep unsteady waves: an efficient computational scheme*. Proc. 19th Int. Conf. Coastal Eng. **1**, 955-967.
- Gibson, M.M. & Rodi, W. (1981) *A Reynolds-stress closure model of turbulence applied to the calculation of a highly curved mixing layer*. J. Fluid Mech. **103**, 161-182.
- Haydon, T.A., Hann, D.B., Davies, P. and Greated, C.A. (1995) *Turbulence Structures in the Surf Zone*. Submitted to ICCE '96.
- Lin, J.C. & Rockwell, D. (1995). *Evolution of a quasi-steady breaking wave*. J.Fluid Mech., **302**, 29-44.
- Lugt, H.J. & Ohring, S. (1992) *The oblique ascent of a viscous vortex pair toward a free surface*. J.Fluid Mech. **236**, 461-476.
- Madsen, P.A. & Svendsen, I.A. (1983) *Turbulent bores and hydraulic jumps*. J. Fluid Mech. **129**, 1-25.
- Moore, D.W. (1978). *The equation of motion of a vortex layer of small thickness*. Stud. Appl. Maths., **58**, 119-140.
- Peregrine, D.H. (1992) *Mechanisms of water-wave breaking*. In Breaking waves. IUTAM Symposium, Sydney. (ed. M.L.Banner & R.H.J. Grimshaw), 39-53.
- Peregrine, D.H. & Svendsen, I.A. (1978) *Spilling breakers, bores and hydraulic jumps*. Proc. 16th Int. Conf. Coastal Eng., 540-550.

Quinn, P.A., Barnes, T., Lloyd, S.T., Greated, C.A. and Peregrine, D.H., (1995), *Velocity Measurements of Post-Breaking Turbulence Generated by Breaking Waves*. Proceedings of Coastal Dynamics '95 Conference, 293-304.

Stansby, P.K. & Slaouti, A. (1984) *On nonlinear wave interaction with cylindrical bodies: a vortex sheet approach*. Appl. Ocean Res., **6**, 108-115.

Svendsen, I.A. & Madsen, P.A. (1984). *A turbulent bore on a beach*. J. Fluid Mech. **148**, 73-96.

Tong, R.P., (1991) *Unsteady Flow with a Free Surface: A Study of Numerical Approximations in the Boundary Integral Method*. Ph.D. Thesis, University of Bristol.